ISSN 0036-0295, Russian Metallurgy (Metally), Vol. 2021, No. 9, pp. 1102–1115. © Pleiades Publishing, Ltd., 2021.
Russian Text © The Author(s), 2021, published in Metally, 2021, No. 5, pp. 70–85.

Superplasticity of High-Strength Submicrocrystalline Al–0.5Mg–Sc Aluminum Alloys

V. N. Chuvil'deev[a, *], M. Yu. Gryaznov[a], S. V. Shotin[a], A. V. Nokhrin[a], V. I. Kopylov[a, b], K. V. Likhnitskii[a], M. K. Chegurov[a], N. Yu. Tabachkova[c, d], A. A. Bobrov[a], and O. E. Pirozhnikova[a]

[a] *Lobachevskii National Research State University of Nizhny Novgorod, Nizhny Novgorod, Russia*
[b] *Physicotechnical Institute, Belarussian Academy of Sciences, Minsk, Belarus*
[c] *Prokhorov General Physics Institute of the Russian Academy of Science, Moscow, Russia*
[d] *National Research University of Science and Technology MISiS, Moscow, Russia*
**e-mail: nokhrin@nifti.unn.ru*

Received January 11, 2021; revised March 22, 2021; accepted April 12, 2021

Abstract—The effect of scandium on the superplasticity characteristics of Al–0.5Mg–Sc conductor aluminum alloys with a submicrocrystalline (SMC) structure is investigated. Large elongation to failure (~1060%) is achieved in the SMC alloys with 0.4 and 0.5% Sc at a deformation temperature of 500°C and a strain rate of 1×10^{-1} s^{-1}. Intense pore formation is shown to occur during the superplasticity of the Al–0.5Mg–Sc SMC alloys. The kinetics of deformation-stimulated grain growth in the Al–0.5Mg–Sc SMC alloys is found to be determined by the mobility of junction disclinations and orientation-misfit dislocations.

Keywords: aluminum, scandium, submicrocrystalline structure, superplasticity, deformation-stimulated grain growth, cavitation

DOI: 10.1134/S0036029521090068

INTRODUCTION

Al–Mg–Sc aluminum alloys have a unique combination of a high strength, corrosion resistance, weldability, and high thermal stability [1–3]. This unique set of properties opens up great prospects for the use of Al–Mg–Sc aluminum alloys in aircraft, automotive engineering, electrical engineering, and so on.

One of the promising ways to further improve the physicomechanical properties of aluminum alloys is the formation of a submicrocrystalline (SMC) structure in them by the method of severe plastic deformation (SPD) [4, 5]. According to [6, 7], high-rate superplasticity effect takes place in Al–Mg–Sc SMC alloys and allows hot deformation to be perforemd at low temperatures and high processing speeds.

Currently, most studies are devoted to the problem of superplasticity of SMC aluminum alloys with a high magnesium content (2–6%), which additionally stabilizes the SMC structure of aluminum and leads to a decrease in the grain-boundary diffusion coefficient [8].[1] The works on the superplasticity of SMC aluminum alloy conductors without magnesium or with an extremely low magnesium content, which negatively affects the electrical conductivity of aluminum, are very scarce, although the problem of optimal hot deformation conditions (drawing or rolling) for wires made of SMC aluminum alloys is very important.

We also note that the problem of the influence of Al_3Sc particles on the superplasticity characteristics of SMC aluminum alloys is still unresolved. At the same time, the positive effect of scandium on the superplasticity characteristics of SMC alloys is well known [6, 7]. Precipitating Al_3Sc nanoparticles prevent intense migration of grain boundaries and, hence, increase the rate of grain-boundary sliding (GBS) [9]. However, the effect of the particles having precipitated in the crystal lattice volume and at grain boundaries on the superplasticity characteristics of SMC alloys can be different, since they differently affect the character of grain growth and, most importantly, the character of fracture.

The purpose of this work is to study the superplastic deformation of Al–0.5Mg–Sc conductor alloys with various scandium contents.

EXPERIMENTAL

Al–0.5Mg–Sc alloys containing 0, 0.2, 0.3, 0.4, and 0.5% Sc were studied. To prepare them, A99 aluminum, Mg90 magnesium, and Al–10% Zr and Al–2% Sc master alloys were used. Alloy samples (22 × 22 × 150 mm in size) were fabricated by induction casting in an INDUTHERM VTC-200 casting

[1] From here on, the element contents are given in wt %.

machine (graphite mold, zirconium oxide crucible, argon atmosphere in melting chamber) according to the following conditions: the initial melt temperature was 710°C, the melt holding time before the introduction of magnesium was 4 min, the magnesium introduction temperature was 750°C, the holding time before casting was 3 min, and the cooling time was 40 s. After casting, the alloys were not quenched and homogenized.

An SMC structure was formed in a billet by equal-channel angular pressing (ECAP) using a Ficep HF400L hydraulic press according to the following conditions: the ECAP temperature was $t_{ECAP} = 225$°C, the strain rate was 0.4 mm/s, the number of cycles was $N = 4$, and the deformation route was B_c (billet was rotated around its axis through an angle of 90° after each ECAP cycle).

A microstructure was studied with a Leica IM DRM metallographic microscope, a Jeol JSM-6490 scanning electron microscope (SEM), and a Jeol JEM-2100 transmission electron microscope (TEM). Polarized illumination was used to identify small details (small pores, "thin" grain boundaries, etc.) on the surface of a polished section during metallographic examination. For microstructure studies, the sample surface was subjected to mechanical polishing with diamond pastes to a roughness level of <1 μm, followed by polishing in a solution 8% $HClO_4$ + 9% H_2O + 10% $C_6H_{14}O_2$ + 73% C_2H_5OH for 15–20 s (voltage was $U \approx 40$ V, current density was $j \approx 3$ A/cm^2). To reveal a microstructure, etching was performed in a glycerin-based solution (1% HF + 1.5% HCl + 2.5% HNO_3 + 95% glycerin); to reveal a macrostructure, etching was performed in a solution 40% HNO_3 + 40% HCl + 20% HF. The average grain size was determined by the chord method using the GoodGrains software package.

Microhardness of $HV_{0.5}$ was measured on an HVS1000 hardness tester. Tensile tests of flat dumbbell test pieces with a gage length of 3 mm and a cross section of 2 × 2 mm were carried out on a Tinius Olsen H25K-S tensile-testing machine (Fig. 1). The holding time in a furnace before a superplasticity experiment was 5 min.

Samples were annealed in an SNOL air furnace and cooling was performed in air.

RESULTS

The as-cast alloys have a homogeneous coarse-grained structure. When the scandium content increases from 0.2 to 0.5%, the average grain size decreases from 1000–1200 to 30–40 μm. The structure of the alloys with a scandium content of >0.3% contains single large light Al_3Sc particles, the average size of which is ~0.35–1.3 μm. The volume fraction of these particles increases the scandium content. After ECAP, a homogeneous SMC structure is formed with

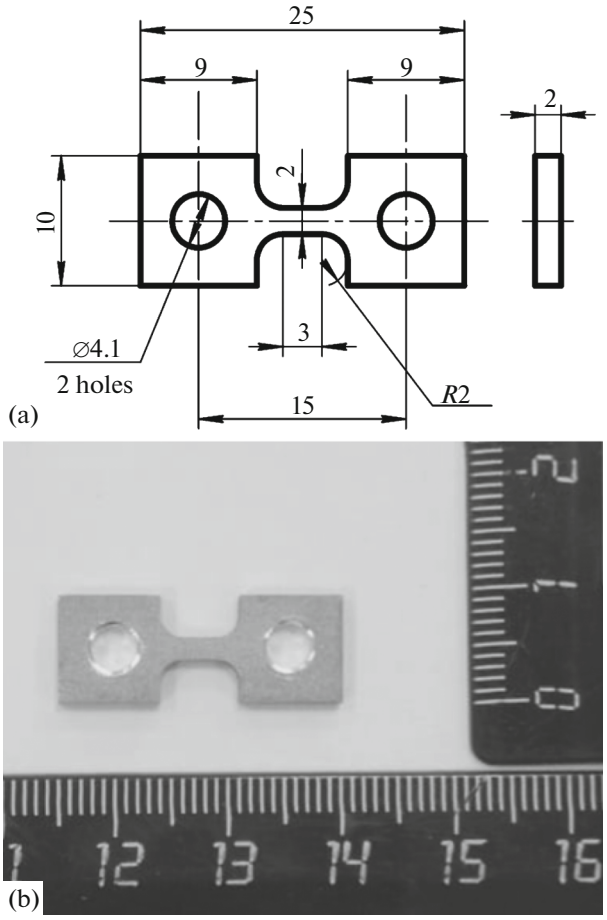

Fig. 1. Tensile test specimen: (a) drawing of the specimen and (b) photo of an aluminum alloy specimen.

an average grain size from 0.8–1 to 0.4–0.5 μm, which does not depend on the scandium content (Fig. 2).[2]

Recrystallization in the Al–0.5% Mg SMC alloy begins after annealing at a temperature $t_1 = 225$°C for 30 min. Scandium alloying leads to an increase in the thermal stability of the Al–0.5% Mg SMC alloy. The temperature of the beginning of recrystallization t_1 in the scandium-alloyed SMC alloys is 375°C; as can be seen from Fig. 3, the average recrystallized grain size decreases with increasing scandium content.

A high level of thermal stability of the SMC structure is provided by the precipitation of Al_3Sc nanoparticles. As was shown in [10], the decomposition of the solid solution in Al–0.5% Mg–Sc SMC alloys is multistage and determined by the intensity of diffusion processes along grain boundaries at "low" annealing temperatures and the intensity of diffusion along lattice dislocation cores at "high" temperatures or long annealing times. In addition, the solid solution in the alloys with a high scandium content (>0.3%) under-

[2] The microstructure of the as-cast and SMC Al–0.5% Mg–Sc alloys was described in detail in [10].

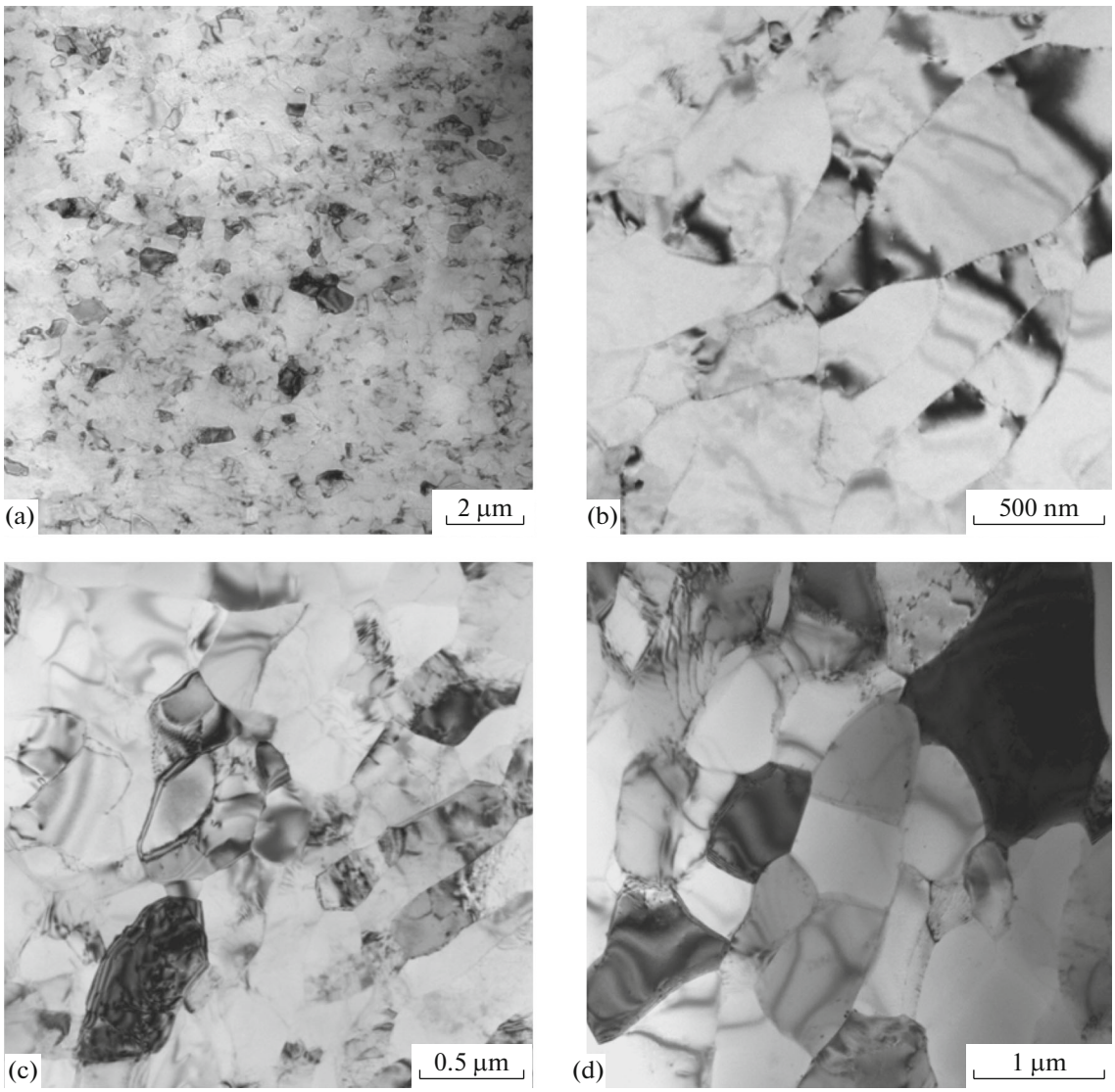

Fig. 2. Microstructure of the SMC alloys (a) Al–0.5Mg, (b) Al–0.5Mg–0.2Sc, (c) Al–0.5Mg–0.3Sc, and (d) Al–0.5Mg–0.5Sc in the state after ECAP. TEM.

goes homogeneous decomposition with the precipitation of Al_3Sc particles in the grain volume at "medium" annealing temperatures.

Electron-microscopic studies showed that several types of Al_3Sc particles precipitate along grain boundaries and in the grain volume in the structure of the Al–0.5% Mg–Sc SMC alloys upon long-term holding. The structure of the alloy also contains elongated particles up to 100–200 nm long, which are perpendicular to grain boundaries, and particles on dislocations and low-angle boundaries, which have a characteristic stitch arrangement.

Figure 4 shows the σ–$\dot{\varepsilon}$ curves for Al–0.5Mg–Sc SMC alloy samples with various scandium contents. The results of superplasticity tests are summarized in Table 1.

The $\sigma(\dot{\varepsilon})$ diagrams presented in Fig. 4 for the SMC alloys at elevated temperatures have the shape characteristic of the superplastic flow of fine-grained aluminum alloys (see [6, 7]): a short stage of strain hardening and a long stage of localized plastic flow. An analysis of the data in Table 1 shows that an increase in the test temperature leads to a monotonic decrease in the flow stress and to a significant increase in the plasticity: at a deformation temperature of 500°C and a strain rate of 1×10^{-2} s^{-1}, the flow stress in the alloy with 0.4% Sc does not exceed $\sigma_b = 6$–8 MPa and the relative elongation reaches $\delta = 840\%$. It is also interesting that scandium alloying increases the degree of uniform deformation. As can be seen from the $\sigma(\dot{\varepsilon})$ curves in Fig. 4a, the degree of uniform deformation in the Al–0.5%Mg SMC alloy is extremely low and the stage of strain hardening almost immediately

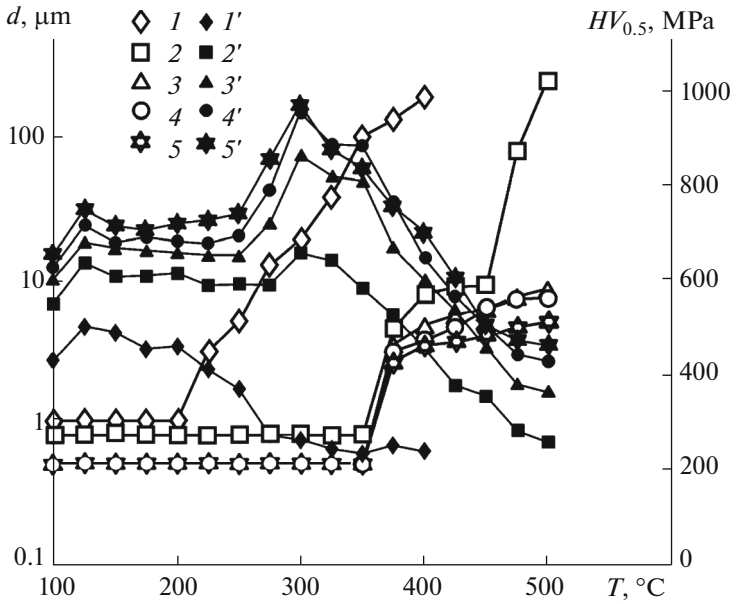

Fig. 3. (*1*–*5*) Average grain size and (*1*'–*5*') microhardness vs. the temperature of 30-min annealing of the Al–0.5Mg–Sc SMC alloys at a scandium content of (*1*, *1*') 0, (*2*, *2*') 0.2, (*3*, *3*') 0.3, (*4*, *4*') 0.4, and (*5*, *5*') 0.5%.

changes into the stage of localized plastic flow. In the SMC alloys with scandium, the degree of uniform deformation at elevated (400–500°C) superplasticity temperatures is quite high (100–150%).

Due to different characters of the σ(ε̇) curves for the Al–0.5% Mg and Al–0.5% Mg–Sc SMC alloys, it is interesting to note the formation of several "necks" during the superplastic flow of the Al–0.5Mg SMC alloy samples: several localized deformation areas are clearly visible in the fracture zone, which are indicated by the arrows in Fig. 5a. The scandium-containing SMC alloy samples have a well-pronounced localized deformation zone regardless of the temperature–rate superplastic deformation conditions (Figs. 5b–5e).

Table 1. Results of superplasticity tests of the Al–0.5Mg–Sc SMC alloys

t, °C	ε̇, s^{-1}	Scandium content in alloy, %									
		0.0		0.2		0.3		0.4		0.5	
		σ_b, MPa	δ, %	σ_b, MPa	δ, %	σ_b, MPa	δ, %	σ_b, MPa	δ, %	σ_b, MPa	δ, %
20	1×10^{-2}	170	45	216	42	221	40	220	38	245	44
300	1×10^{-2}	47	165	65	160	59	205	56	225	57	345
350	1×10^{-2}	27	210	33	290	32	295	28	280	33	320
400	1×10^{-3}	9	290	9	275	7	510	10	250	11	290
	3×10^{-3}	12	290	10	560	12	490	12	350	13	260
	1×10^{-2}	18	240	20	350	18	425	17	460	21	480
	3×10^{-2}	19	265	24	290	20	360	23	320	23	680
450	1×10^{-2}	12	275	13	350	10	490	10	500	14	400
500	1×10^{-3}	4	340	4	400	4	540	4	330	4	520
	3×10^{-3}	6	330	8	265	5	820	4	530	5	670
	1×10^{-2}	8	280	9	350	6	625	8	840	7	750
	3×10^{-2}	10	270	14	220	13	400	7	1060	9	1055
	1×10^{-1}	–	–	–	–	–	–	15	500	–	–

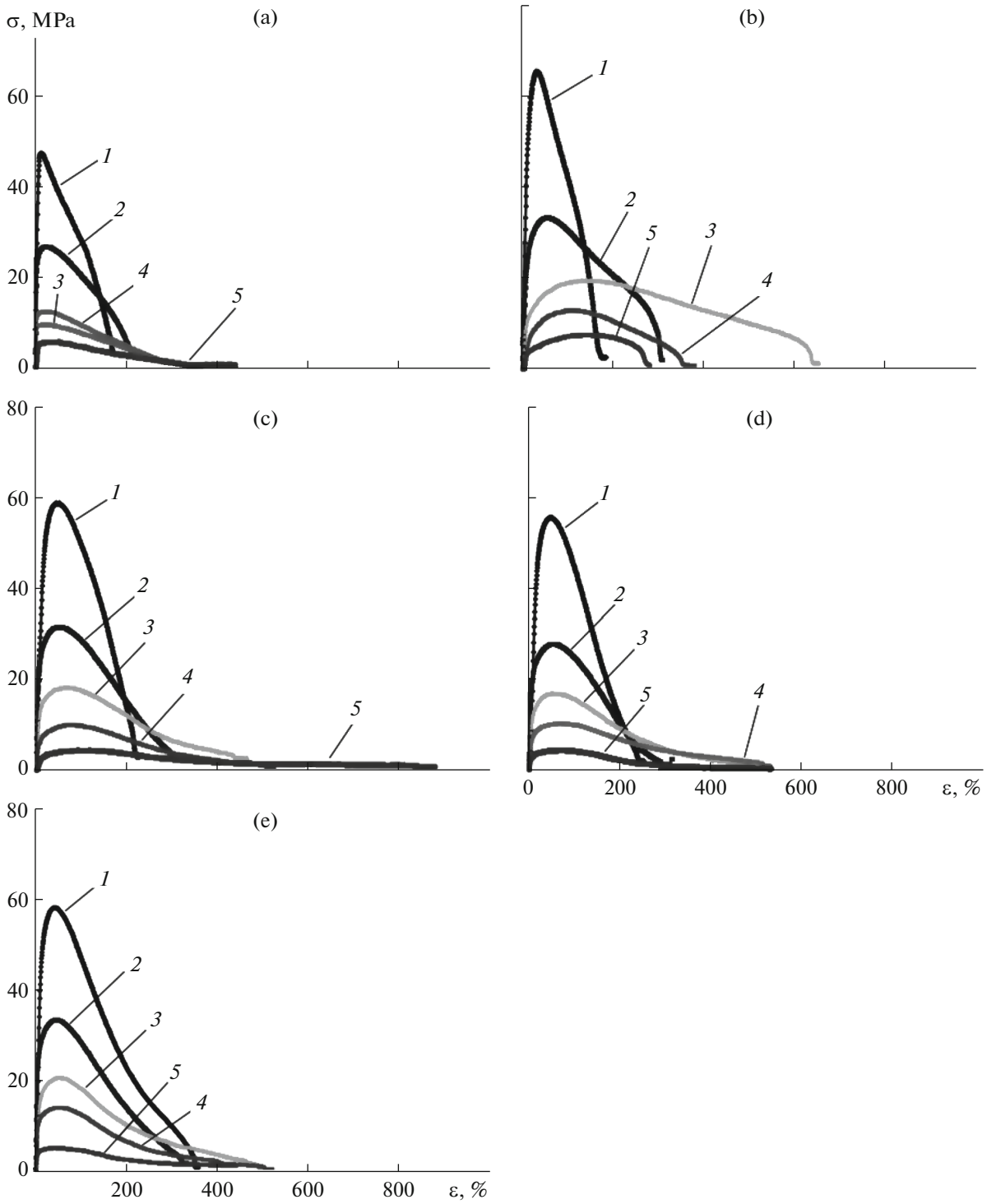

Fig. 4. Stress (σ)–strain (ε̇) curves for the Al–0.5Mg–Sc alloys (with (a) 0, (b) 0.2, (c) 0.3, (d) 0.4, (e) 0.5% Sc) at a test temperature t = (*1*) 300, (*2*) 350, (*3*) 400, (*4*) 450, and (*5*) 500°C) and a strain rate of 1×10^{-2} s^{-1}.

Strain-rate sensitivity m, which is determined from the slope of the flow stress curve as a function of the strain rate in the $\log\sigma_u$–$\log\dot{\varepsilon}$ logarithmic coordinates, depends nonmonotonically on the scandium content: it increases from 0.22 (Al–0.5Mg alloy) to 0.32 (alloy with 0.3% Sc) at a deformation temperature of 400°C and decreases again to ~0.21–0.22 when the scandium content increases to 0.5%. A similar character of the m(Sc) dependence is also observed at a deformation temperature of 500°C: when the scandium content

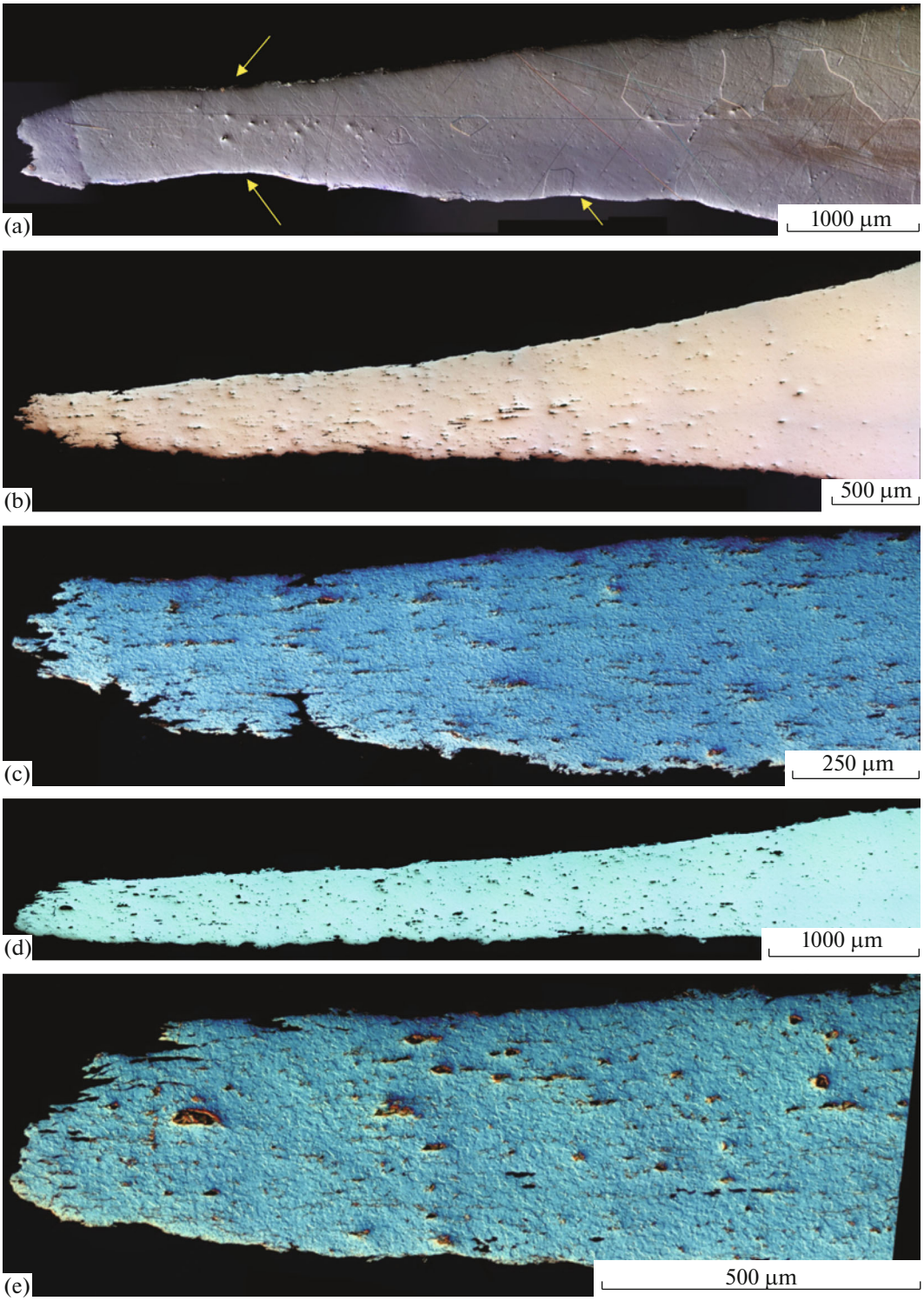

Fig. 5. Macrostructure of Al–0.5Mg–Sc SMC alloy samples after superplasticity tests at a scandium content of (a) 0% ($t = 500$°C, $\dot{\varepsilon} = 1 \times 10^{-3}$ s^{-1}), (b, c) 0.3% ($t = 400$°C, $\dot{\varepsilon} = 3.3 \times 10^{-3}$ s^{-1}), and (d, e) 0.3% ($t = 500$°C, $\dot{\varepsilon} = 3.3 \times 10^{-3}$ s^{-1}). (c, e) Enlarged images of the fracture surfaces of the samples, the photographs of which are shown in (b) and (d), respectively.

increases from 0 to 0.3%, coefficient m increases from 0.24–0.25 to 0.35–0.36; when the scandium content increases to 0.5%, it monotonically decreases to 0.19–0.20. Note that the maximum values of coefficient m are quite low and do not reach the optimum value ($m = 0.5$), although a very large elongation to failure is

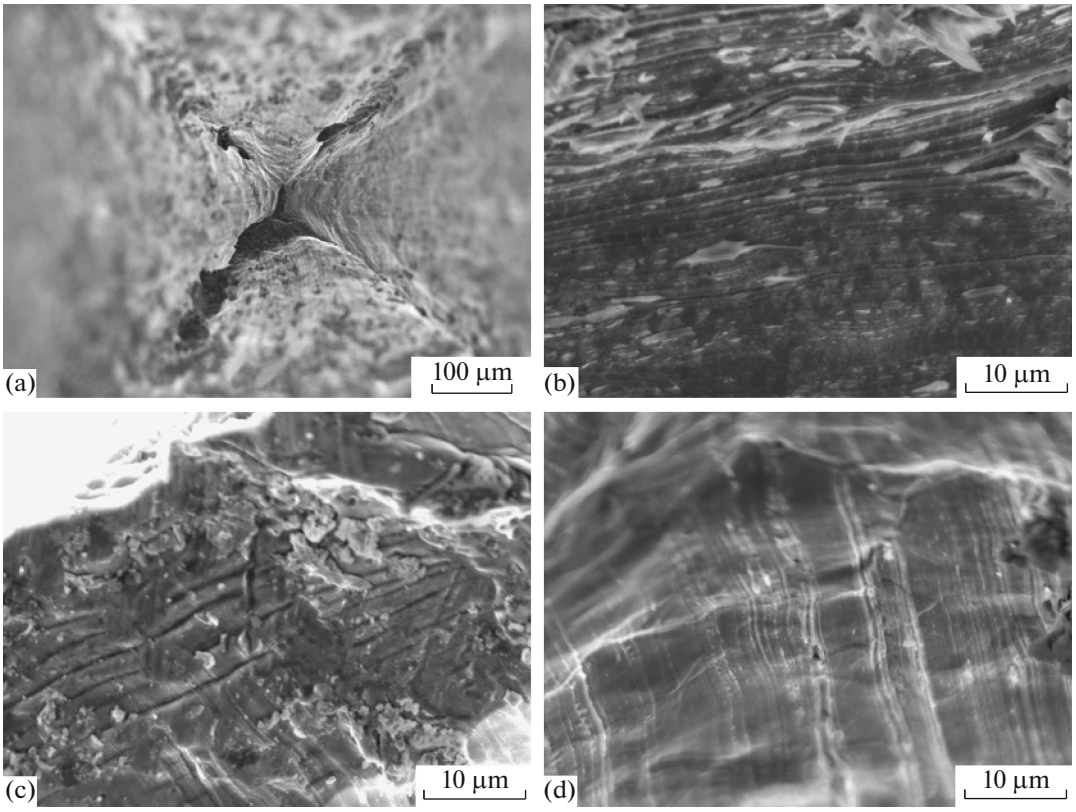

Fig. 6. (a–d) Fractographs of the fracture surfaces of the Al–0.5Mg SMC alloy samples tested at a temperature of 400°C and a strain rate $\dot{\varepsilon} = 1 \times 10^{-2}$ s^{-1}; (b–d) enlarged images of the fracture zone. SEM.

achieved in the SMC alloys containing 0.4 and 0.5% Sc at a temperature of 500°C and a strain rate of 1×10^{-1} s^{-1}, (~1060%; see Table 1). Coefficient m nonmonotonically, with a maximum, depends on the strain rate, and the strain rates at which m and elongation to failure are maximal are close to each other.

Metallographic analysis of the macrostructure of the failed Al–0.5Mg–Sc samples reveals a high volume fraction of large pores near the fracture zone, and the pore size ranges from 2–3 to 5–20 μm (Figs. 5b–5e). The volume fraction of pores correlates with the strain to failure: the higher the strain to failure, the larger the size and volume fraction of pores near the fracture zone. Note that large pores are almost absent in the Al–0.5% Mg SMC alloy samples (see Fig. 5a). This fact suggests that the source of pore formation during superplasticity tests is primarily the large Al_3Sc particles having formed during the solidification of ingots or during the decomposition of a solid solution.

Fractographic analysis of the fracture surfaces of the Al–0.5Mg SMC alloy samples subjected to superplasticity tests shows that the rupture zone occupies almost the entire fracture area (Fig. 6). The fracture of the Al–0.5Mg–0.3Sc SMC alloy samples has a viscous character, and numerous dimples formed as a result of micropore coalescence are observed in the fracture surfaces of the samples (Fig. 7). A high volume fraction of micropores in the fracture surfaces indicates accelerated cavitation fracture during the superplasticity of the SMC of alloys with scandium. As can be seen from Fig. 7, an increase in the deformation temperature weakly affects the dimple size: the fracture surfaces of the samples tested at 300 and 500°C are similar to each other.

Metallographic studies of the structure of the Al–0.5Mg samples in the undeformed area (grip region) demonstrate that an increase in deformation temperature from 300 to 500°C leads to rapid grain growth in this part of the samples from 11 to ~190 μm (Fig. 8, Table 2). In testing the SMC alloy samples with scandium, no significant grain growth is observed in the deformed part and the material has a homogeneous fine-grained structure (Fig. 9, Table 2).

Note also that, according to Table 2, the evolution of the structure during the superplasticity of the SMC aluminum alloys with scandium differs from the structure evolution in the Al–0.5Mg SMC alloy. The average grain size in the deformed part of the Al–0.5Mg SMC alloy samples is 1.5–2 times smaller than that in the undeformed part of the samples; that is, the grain structure refinement during superplasticity is likely to be associated with dynamic recrystallization (see [11]).

Deformation-stimulated grain growth is observed during the superplasticity of the SMC alloys with

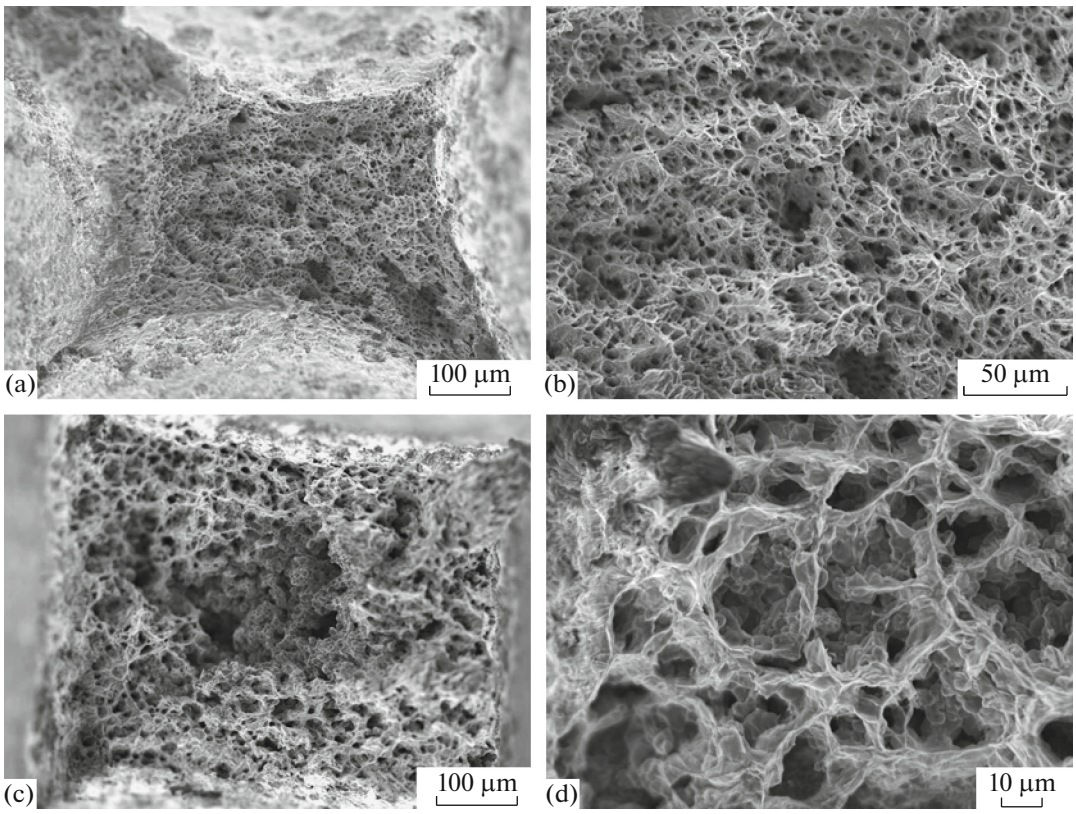

Fig. 7. Fractographs of the fracture surfaces of the Al–0.5Mg–0.3Sc SMC alloy samples tested at a temperature of (a, b) 300 and (c, d) 500°C. The strain rate is $\dot{\varepsilon} = 1 \times 10^{-2}$ s^{-1}. SEM.

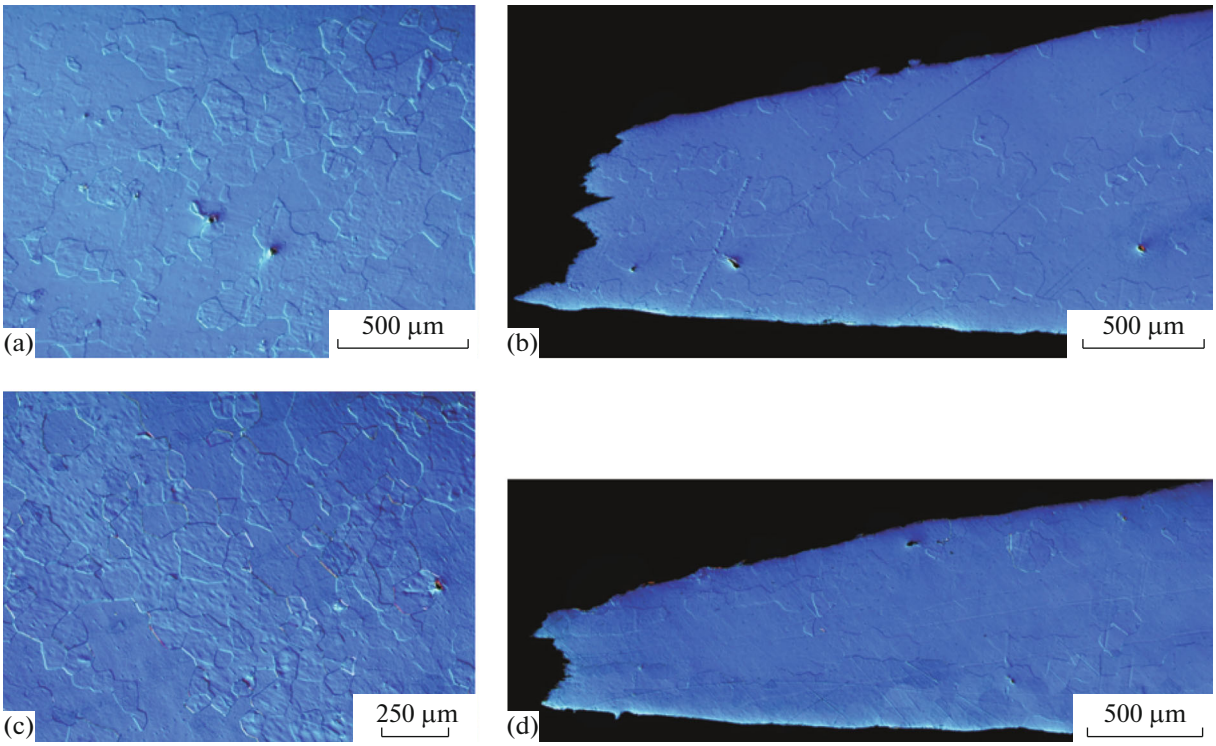

Fig. 8. Microstructures of (a, c) undeformed and (b, d) deformed regions in the Al–0.5Mg SMC samples after superplasticity tests at a strain rate of (a, b) 3.3×10^{-3} and (c, d) 1×10^{-3} s^{-1} and a deformation temperature $t = 400$°C.

Table 2. Results of studying the deformation-stimulated grain growth in the Al–0.5Mg–Sc SMC alloys

t, °C	$\dot{\varepsilon}$, s^{-1}	Scandium content in alloy									
		0.0		0.2		0.3		0.4		0.5	
		d_1	d_2	d_1	d_2	d_1	d_2	d_1	d_2	d_1	d_2
		μm		μm		μm		μm		μm	
20	1×10^{-2}	0.8	0.8	0.4–0.5	0.4–0.5	0.4–0.5	0.4–0.5	0.4–0.5	0.4–0.5	0.4–0.5	0.4–0.5
300	1×10^{-2}	10.9	6.7	0.4–0.5	0.4–0.5	0.4–0.5	0.4–0.5	0.4–0.5	1.5	0.4–0.5	0.4–0.5
350	1×10^{-2}	22.3	13.6	0.4–0.5	2.5	0.4–0.5	2.1	0.4–0.5	2.0	0.4–0.5	1.9
400	1×10^{-3}	76.3	61.5	1.5	4.8	1.3	3.3	1.2	3.1	1.2	3.1
	3×10^{-3}	69.7	57.2	1.3	4.1	1.2	2.9	1–1.2	2.9	1–1.2	2.6
	1×10^{-2}	49.6	29.1	0.8–1.2	3.4	0.8–1	2.7	0.5	2.2	0.5	2.2
	3×10^{-2}	45.6	20.3	0.7	2.8	0.5	2.6	0.5	2.1	0.5	2.1
450	1×10^{-2}	111.5	59.9	1.7	4.2	1.2	3.6	1.2	2.8	1–1.2	2.4
500	1×10^{-3}	402.7	287.9	2.5	10.3	2.1	8.0	1.5	6.0	1.2	4.5
	3×10^{-3}	293.9	267.0	2.2	8.8	1.7	5.6	1.2	5.3	1.2–1.3	3.6
	1×10^{-2}	223.6	102.7	2.0	7.8	1.5	4.5	1.0	4.6	1.0	3.5
	3×10^{-2}	188.7	—	0.5	5.6	0.5	3.3	0.5	3.9	0.5	3.2

d_1 and d_2 are the average grain sizes in the undeformed and deformed regions of the samples, respectively, after superplasticity tests.

scandium: the average grain size in the fracture region is larger than that in the undeformed region (see Fig. 9). As follows from Table 2, an increase in the test temperature from 300 to 500°C leads to rapid grain growth in the Al–0.5Mg–Sc SMC alloy samples, and the average grain size in the deformed region (d_2) in the SMC scandium-containing alloys is more than an order of magnitude larger than that in the undeformed region (d_1; see Fig. 9, Table 2). The first recrystallized micrograins in the deformed part of the Al–0.5Mg–Sc SMC alloy samples are observed after tests at 350°C. At a test temperature of 300°C, the alloys after superplasticity tests retain a stable SMC structure. An increase in strain rate from 1×10^{-3} to 3×10^{-2} s^{-1} leads to a slight decrease in the average grain size in the Al–0.5% Mg–Sc SMC alloys at all scandium contents under study (see Table 2).

Note also that, when the scandium content increases, the average grain size in the deformed part of the sample decreases at all superplastic deformation temperatures (see Table 2).

Figure 10 shows the microhardness versus the deformation temperature for the SMC alloys with various scandium contents. The generalized $HV_{0.5}(t)$ dependences demonstrate that the microhardness of the metal in the deformed zone is slightly lower than that in the undeformed zone. The $HV_{0.5}(t)$ dependences for the undeformed region of the SMC alloys with scandium are nonmonotonic two-stage character with a maximum at $t = 350$°C. An increase in the hardness at 350°C is obviously due to the precipitation of Al_3Sc particles, which confirms the closeness of the temperatures of the maxima in the $HV_{0.5}(t)$ dependences for the samples after annealing for 30 min (see Fig. 3) and for the undeformed part of the SMC alloy samples. An analysis of the $HV_{0.5}(t)$ dependences demonstrates that an increase in the deformation temperature leads to a decrease in the microhardness of the deformed part of the Al–0.5% Mg–Sc SMC alloy samples.[3]

The dependence of the microhardness on the grain size (Fig. 11) with a fairly good accuracy is described by the Hall–Petch relation $HV_{0.5} = HV_0 + Kd^{-1/2}$, where HV_0 is the microhardness of the crystal lattice of the SMC metal and K is the grain-boundary hardening coefficient (Hall–Petch coefficient). It is interesting to note that coefficient K depends on the scandium content in an SMC alloy. When the scandium content increases from 0.2 to 0.5%, coefficient K increases from 0.36 to 1.1 MPa $m^{1/2}$. Since K characterizes the contribution of grain boundaries to the hardening of polycrystal [12–14], the revealed dependence K(Sc) is thought to indicate that Al_3Sc particles precipitate mainly at grain boundaries of an SMC alloy during superplastic deformation.

DISCUSSION

To describe the deformation-stimulated grain growth in the SMC aluminum alloys, we use the

[3] The fact that $HV_{0.5}$ does not depend on the annealing temperature and the grain size for the Al–0.5% Mg SMC alloy is mainly caused by the small indentation size, which is comparable with the grain size during intense grain growth.

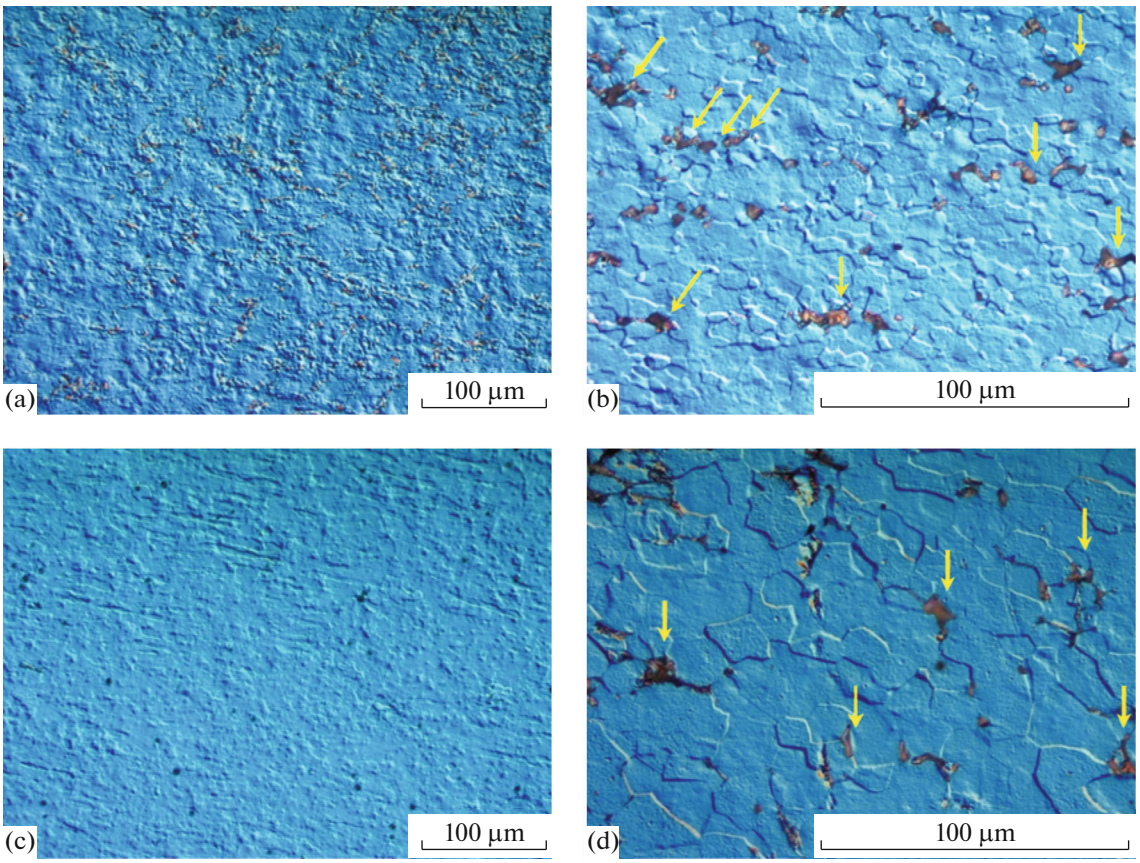

Fig. 9. Microstructure of undeformed (a, c) and deformed (b, d) regions in Al–0.5Mg–0.2Sc SMC samples after superplasticity tests at (a, b) $t = 400°C$ and $\dot{\varepsilon} = 1 \times 10^{-3}$ s^{-1} and (c, d) $t = 500°C$ and $\dot{\varepsilon} = 1 \times 10^{-3}$ s^{-1}. The arrows in (b) and (d) indicate the pores formed on the Al_3Sc particles.

approach developed in terms of the theories of structural superplasticity [15, 16] and nonequilibrium grain boundaries in metals [17]. In this approach, systems of disclination dipoles, which create long-range stress fields σ_i, exert a decisive effect on the grain growth in fine-grained materials. The interaction of the dipoles with each other causes an additional driving force of migration P_ω. In addition, defects also affect the diffusion mobility of grain boundaries M; at a high strength of the disclination dipoles, it can be limited by their mobility M_ω.

When the dislocation and disclination defects distributed in a grain boundary interact with external (σ) and internal (σ_i) stress fields, the following additional driving forces of grain-boundary migration arise [17]:

$$\begin{aligned} P &= (\sigma + \sigma_i)(\rho_b \Delta b + \omega) \\ &= \bar{\sigma}(\rho_b \Delta b + \omega) = P_\rho + P_\omega, \end{aligned} \quad (1)$$

where σ_i is the internal stress field created by the defects distributed at grain boundaries and triple junctions of grain boundaries,

$$\sigma_i = \alpha_1 G \rho_b^{st} \Delta b + \alpha_2 G \omega. \quad (2)$$

In Eqs. (1) and (2), $\bar{\sigma}$ is the mean internal stress field, P_ρ is the driving force related to the orientation-misfit dislocations (OMDs), G is the shear modulus, ρ_b^{st} is the stationary OMD density in nonequilibrium grain boundaries of an SMC metal, Δb is the Burgers vector of OMDs, and α_1 and α_2 are numerical coefficients.

In this case, the effective grain-boundary mobility coefficient is determined from the expression [17]

$$M^{-1} = M_b^{-1} + M_\rho^{-1} + M_\omega^{-1}, \quad (3)$$

where M_b is the mobility coefficient of a defect-free grain boundary, M_ρ is the mobility coefficient of the OMDs distributed in the grain boundary, and M_ω is the mobility coefficient of a junction disclination. We have

$$\begin{aligned} M_\rho = A_\rho C_b \frac{b}{d}\frac{b}{G}\frac{1}{\rho_b^{st}\Delta b}, \quad M_\omega = A_\omega C_b \left(\frac{b}{d\omega}\right)^2 \frac{b}{G}, \\ M_b = A_b C_b \left(\frac{b}{d}\right)^2 \frac{b}{G}, \end{aligned} \quad (4)$$

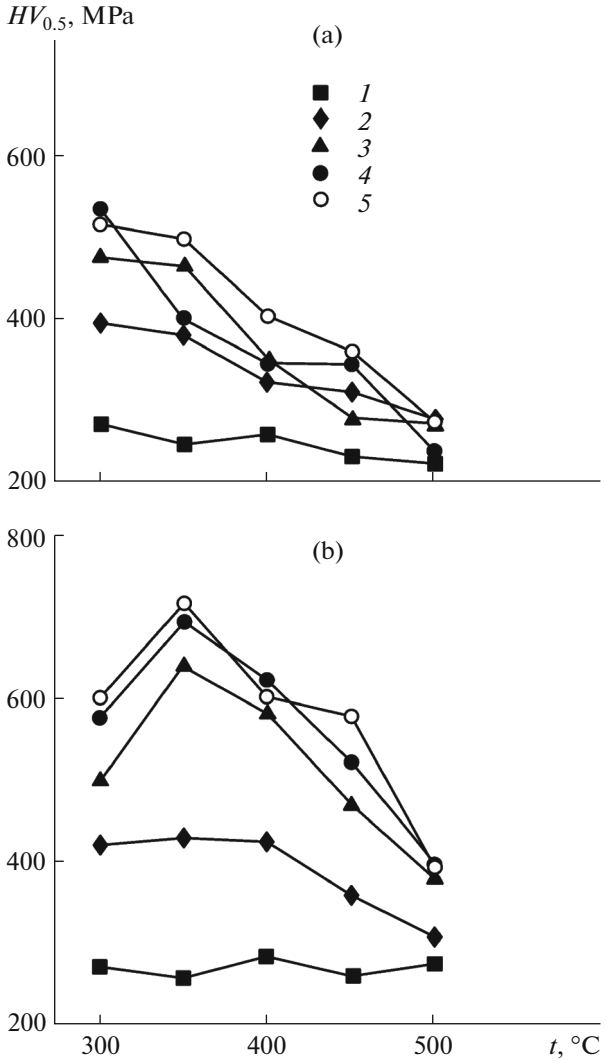

Fig. 10. Microhardnesses of (a) deformed and (b) undeformed regions in the SMC alloys (*1*) Al–0.5Mg, (*2*) Al–0.5Mg–0.2Sc, (*3*) Al–0.5Mg–0.3Sc, (*4*) Al–0.5Mg–0.4Sc, and (*5*) Al–0.5Mg–0.5Sc vs. the temperature of superplastic deformation at a rate of 1×10^{-2} s^{-1}.

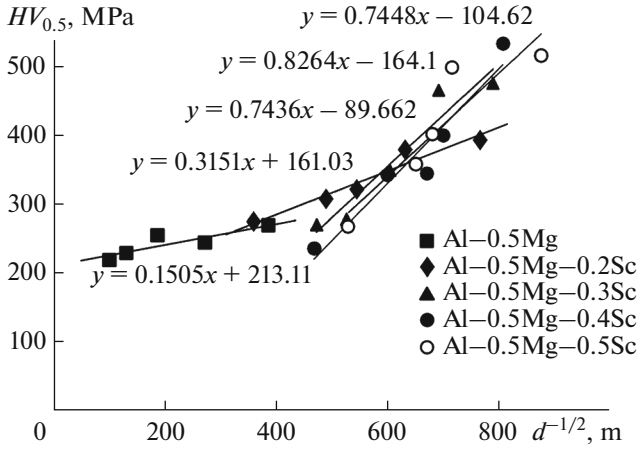

Fig. 11. Microhardness vs. the grain size in the $HV_{0.5}$–$d^{-1/2}$ coordinates (analysis of the results presented in Fig. 10 and in Table 2).

where $C_b = G\delta D_b/k_B T$, $A_\rho = 2\pi/\ln(d/b)$, $A_\omega \approx 1$, $A_b = (5V_m/\Delta b)(d_0/b)^4(Gb/\gamma_b)$, V_m is the experimental grain growth rate during annealing, $\delta = 2b$ is the grain boundary width, b is the Burgers vector, D_b is the grain-boundary diffusion coefficient, k_B is the Boltzmann constant, and γ_b is the grain boundary energy.

The grain-boundary migration rate V_g under superplastic deformation with allowance for Eqs. (3) and (4) can be written as follows:

$$V_g = \frac{M_b M_\rho M_\omega}{M_b M_\rho + M_b M_\omega + M_\rho M_\omega}\bar{\sigma}\left(\rho_b^{st}\Delta b + \omega\right). \quad (5)$$

As follows from Eq. (5), the kinetics of deformation-stimulated grain growth in fine-grained alloys is complex and depends primarily on the grain-boundary migration mobility, the mobility of the defects distributed in a grain boundary, the strength of a dipole of junction disclinations, and the OMD density. At a low strength ω of the junction disclinations, the grain boundary mobility is determined by the OMD mobility, and the driving force is associated with the interaction of OMDs with an external stress field [18],

$$V_g = \dot{d} = A_\rho C_b\left(\sigma/G\right)\left(b/d\right)b. \quad (6)$$

In the case of high values of ω, the grain-boundary mobility during superplasticity is controlled by the disclination dipole mobility, and the driving force is related to their interaction [18],

$$V_g = \dot{d} = A_\omega C_b\left(b/d\right)^2 b. \quad (7)$$

In the case of average values of ω, the rate of deformation-stimulated grain growth can be expressed in a more general form

$$\dot{d} = A\left(d/b\right)^{-x},$$

where $A \cong C_b b(\sigma/G)^{2-x}$, and exponent x takes values from 1 to 2 depending on junction disclination strength ω. For low values of ω, we have $x = 1$ and $A = A_\rho C_b b(\sigma/G)$; for high values of ω, we have $x = 2$ and $A = A_\omega C_b$.

The analysis carried out in [18] showed that the initial grain size exerts a significant effect on the deformation-stimulated growth under given superplasticity test conditions. For small grain sizes (in the case of SMC materials), the driving force of grain-boundary migration is caused by the interaction of external stresses with the OMDs distributed in a grain boundary, and the expression for the grain growth rate has the form of Eq. (7). According to [18], the critical grain size d^* at which the mechanism of deformation-

stimulated grain growth changes can be calculated by the formula

$$d^* = \left[(\sigma/G)(C_b/\xi\dot{\varepsilon}_v)\right]^{1/3},$$

where ξ is the numerical parameter that characterizes the degree of deformation uniformity.

The experimental dependence of the grain growth rate on the strain rate is usually expressed in the form $\dot{d} \sim \dot{\varepsilon}^k$, where parameter k, which depends on strain rate $\dot{\varepsilon}$, is determined from the slope of the curve $\log\dot{d}$–$\log\dot{\varepsilon}$ at a fixed strain. As can be seen from Fig. 12, the experimental value of the coefficient (k_{exp}) for the Al–0.5Mg–Sc SMC alloys at 400°C increases slightly from ~0.8 to ~1.3 when the scandium content increases from 0.2 to 0.5%. At a deformation temperature of 500°C, k_{exp} weakly depends on the scandium content, $k_{exp} \approx 0.6$–1.

According to [18], the theoretical expression for the parameter k_{th}, $k_{th} = \partial\log\dot{d}/\partial\log\dot{\varepsilon}$, has a cumbersome form in the general case. For the case of fine-grained alloys, the expression for k_{th} with allowance for the expression $\dot{\varepsilon} \sim A\sigma^{1/m}d^{-p}$ has the form

$$k_{th} = m + \frac{\partial m}{\partial\log\dot{\varepsilon}}\frac{1}{m}\left[pm\log\frac{d_0}{b} + \log\frac{\sigma}{G}\right] + (pm-1)\frac{\partial\log(d/b)}{\partial\log\dot{\varepsilon}}, \quad (8)$$

$$d(t)^2 - d_0^2 = C_b b^2(\sigma/G)\tau,$$

where τ is the deformation time, p is the exponent of the grain size, and d_0 is the initial grain size.

For coarse-grained materials, the formula for calculating k_{th} has the form [18]

$$k_{th}^2 = \frac{2}{3}\frac{C_b(b/d_0)^3}{1 + C_b(b/d_0)^3 t}. \quad (9)$$

A comparison of the experimental (k_{exp}) and theoretical (k_{th}) parameters demonstrates that the kinetics of deformation-stimulated grain growth in coarse-grained alloys with a low scandium content is mainly controlled by the junction disclination mobility and this kinetics in fine-grained alloys with a high scandium content is controlled by the OMD mobility (Table 3).

The differences between the experimental (k_{exp}) and theoretical (k_{th}) parameters are thought to be primarily due to the fact that the model [18] did not take into account the influence of second-phase particles on the grain growth kinetics. As is known [19, 20], the grain growth in fine-grained alloys with particles can be described by a power law with an exponent other than $p = 2$.

In conclusion, we briefly touch on the causes of the cavitation fracture of the SMC alloys with scandium.

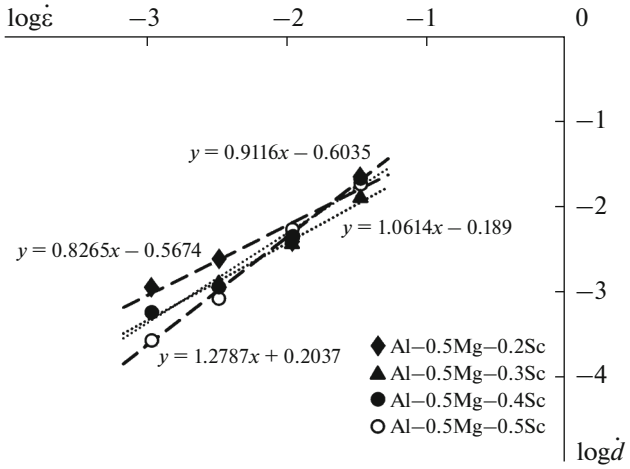

Fig. 12. Rate of the deformation-stimulated grain growth vs. the superplastic deformation rate in the $\log\dot{d}$–$\log\dot{\varepsilon}$ logarithmic coordinates. The deformation temperature is 400°C.

A model for the formation of pores on second-phase particles located in the triple junctions of grains under superplasticity was proposed in [21]. According to this model, the formation of pores in the triple junctions of grain boundaries is caused by the accumulation of the normal components of delocalized dislocations, which lead to the appearance of a defective layer at the particle/matrix interface, the energy and internal stresses of which increase during superplastic deformation.

As was shown above, large Al_3Sc particles can precipitate during heating or solidification, and some of them are located along grain boundaries. The fact of pore formation along grain boundaries is quite clearly illustrated by Fig. 7, which shows that the vast majority of pores are located at grain boundaries or in the triple junctions of grain boundaries. The cutting of such particles by lattice dislocations is difficult, and defects of the disclination type will form around them during superplastic deformation. The authors of [22] described these defects in detail and showed that the defect that forms on a particle of radius R located in a grain boundary during deformation can be described in a first approximation as a disclination loop of radius R and strength $\omega(\tau)$. The disclination loop strength $\omega(\tau)$ increases in proportion to the number of defects reaching the grain boundary. In the case when defects reach grain boundaries due to intragrain deformation carried out at rate $\dot{\varepsilon}_v$, the strength of disclination loop at the initial stage of its formation can be calculated by the formula $\omega(t) = \psi_1\dot{\varepsilon}_v\tau$ [18], where ψ_1 is the geometric coefficient and $\dot{\varepsilon}_v$ is the rate of intragrain deformation. As defects accumulate at grain boundaries, disclination loop strength $\omega(t)$ increases, and the elastic energy related to this defect also increases. As shown in [21], at a certain critical strength ω^*, the excess

Table 3. Experimental and theoretical values of coefficient k for the Al–0.5Mg–(0.2, 0.5)Sc SMC alloys

t, °C	$\dot{\varepsilon}$, s^{-1}	m	d_1, μm	σ, MPa	d_2, μm	k_{th}		k_{exp}
						Eq. (8)	Eq. (9)	
Al–0.5Mg–0.2Sc alloy								
400	1×10^{-3}	0.18	1.5	9	4.8	0.34	0.69	0.8
	3×10^{-3}	0.21	1.3	10	4.1			
	1×10^{-2}	0.32	0.8–1.2	20	3.4			
	3×10^{-2}	0.10	0.7	24	2.8			
500	1×10^{-3}	0.19	2.5	4	10.3	0.32	0.65	1.0
	3×10^{-3}	0.24	2.2	8	8.8			
	1×10^{-2}	0.25	2.0	9	7.8			
	3×10^{-2}	0.24	0.5	14	5.6			
Al–0.5Mg–0.5Sc alloy								
400	1×10^{-3}	0.10	1.2	11	3.1	0.70	0.32	1.3
	3×10^{-3}	0.11	1–1.2	13	2.6			
	1×10^{-2}	0.41	0.5	21	2.2			
	3×10^{-2}	0.16	0.5	23	2.1			
500	1×10^{-3}	0.11	1.2	4	4.5	0.74	0.34	0.8
	3×10^{-3}	0.12	1.2–1.3	5	3.6			
	1×10^{-2}	0.19	1.0	7	3.5			
	3×10^{-2}	0.28	0.5	9	3.2			

energy of the loop becomes so high that it is energetically favorable for a grain boundary to "become free" of the source of this energy. At elevated temperatures, the deformation of the "relaxation" of the stored energy can occur via micropore formation at Al_3Sc particle/aluminum interphase boundaries. During superplastic deformation, pore growth is proportional to the degree and rate of intragrain deformation [21], and such pores become a source of fracture of an SMC alloy when their critical size is reached.

Thus, under superplastic deformation, large Al_3Sc particles located along grain boundaries in an SMC alloy can be a source of micropore formation and, hence, the cause of cavitation fracture of the Al–0.5Mg–Sc SMC alloys. This finding makes it possible to recommend choosing the annealing or hot deformation conditions that would cause the predominant precipitation of Al_3Sc nanoparticles in the crystal lattice volume for stabilizing a fine-grained structure in Al–0.5Mg–Sc alloys.

CONCLUSIONS

(1) SMC Al–0.5Mg–Sc conductor alloys have high superplastic characteristics: large elongation to failure (~1060%) is achieved in the SMC alloys with 0.4 and 0.5% Sc at a deformation temperature of 500°C and a strain rate of 1×10^{-1} s^{-1}.

(2) The Al–0.5Mg SMC alloy has low thermal stability, and intense grain growth occurs in it to grain sizes of several hundred microns during preliminary heating to the superplastic deformation temperature. This fact does not allow us to provide high superplastic characteristics of the alloy at elevated deformation temperatures. During superplastic deformation, the SMC alloy undergoes ductile fracture without intense pore formation. The average grain size in the fracture region turns out to be smaller than that in the undeformed region, which can be considered as an indirect proof of dynamic recrystallization.

(3) During superplastic deformation of the of Al–0.5Mg–Sc SMC alloys, deformation-stimulated grain growth at parameter $k = \partial \log \dot{d} / \partial \log \dot{\varepsilon}$, which varies from 0.8 to 1.3 depending on the scandium content, is observed. In the alloys with a low scandium content, the kinetics of deformation-stimulated grain growth was found to be controlled by the junction disclination mobility; in the alloys with a high scandium content, by the OMD mobility.

(4) During superplastic deformation of the Al–0.5Mg–Sc SMC alloys, intense pore formation was observed on Al_3Sc particles, which precipitated during

heating and/or solidification. Coarse Al_3Sc particles located along grain boundaries are thought to be the most preferable sites for micropore formation and accelerated fracture. As a result, the cavitation fracture mechanism takes place. Fractographic analysis of the fracture surfaces indicates the presence of a high volume fraction of pores, which caused the fracture of the Al–0.5Mg–Sc SMC alloys.

ACKNOWLEDGMENTS

We thank V.V. Zakharov (AO All-Russia Institute of Light Alloys) for his recommendations on the choice of aluminum alloy casting conditions.

FUNDING

This work was supported by the Russian Science Foundation, project no. 18-13-00306.

REFERENCES

1. V. I. Elagin, *Alloying of Deformable Aluminum alloys with Transition Metals* (Metallurgiya, Moscow, 1975).
2. V. V. Zakharov, "Effect of scandium on the structure and properties of aluminum alloys," Metal Science and Heat Treatment **45** (7–8), 246–253 (2003).
3. V. I. Elagin, V. V. Zakharov, and T. D. Rostova, "Some features of the decomposition of the solid solution of scandium in aluminum," Metal Science and Heat Treatment **25** (7), 546–549 (1983).
4. V. N. Chuvildeev, A. V. Nokhrin, I. M. Makarov, et al., "Solid solution decomposition mechanisms in cast and microcrystalline Al–Sc alloys: I. Experimental studies," Russian metallurgy (Metally), No. 5, 415–427 (2012).
5. S. V. Dobatkin, V. V. Zakharov, A. Yu. Vinogradov, et al., "Nanocrystalline strucutre formation in Al–Mg–Sc alloys during severe plastic deformation," Russian Metallurgy (Metally), No. 6, 533–540 (2006).
6. N. F. Yunusova, R. K. Islamgaliev, and R. Z. Valiev, "High-strain-rate superplasticity in aluminum 1420 and 1421 alloys subjected to equal-channel angular pressing," Russian Metallurgy (Metally), No. 2, 123–128 (2004).
7. V. N. Perevezentsev, V. N. Chuvil'deev, V. I. Kopylov, A. N. Sysoev, and T. G. Langdon, "High-strain-rate superplasticity of Al–Mg–Sc–Zr alloys," Russian Metallurgy (Metally), No. 1, 28–35 (2004).
8. T. Fujita, Z. Horita, and T. G. Langdon, "Characteristics of diffusion in Al–Mg alloys with ultrafine grain sizes," Phil. Mag. A **82**, 2249–2262 (2002).
9. I. I. Novikov and V. K. Portnoi, *Superplasticity of Ultrafine Grain Alloys* (Metallurgiya, Moscow, 1981).
10. V. N. Chuvil'deev, Ya. S. Shadrina, A. V. Nokhrin, V. I. Kopylov, A. A. Bobrov, M. Yu. Gryaznov, S. V. Shotin, N. Yu. Tabachkova, A. V. Piskunov, M. K. Chegurov, and N. V. Melekhin, "Thermal stability of the structure and mechanical properties of submicrocrystalline Al–0.5%Mg–Sc aluminum alloys," Russ. Metall. (Metally), No. 1, 7–24 (2021).
11. I. I. Novikov, V. K. Portnoy, A. O. Titov, and D. Yu. Belov, "Dynamic recrystallization at superplastic deformation of duraluminum with initial recrystallized structure," Scr. Mater. **42** (9), 899–904 (2000).
12. V. N. Chuvil'deev, A. V. Nokhrin, M. M. Myshlyaev, V. I. Kopylov, et al., "Effect of recovery and recrystallization on the Hall-Petch relation parameters in submicrocrystalline metals: I. Experimental studies," Russ. Metall. (Metally), No. 1, 71–89 (2018).
13. V. N. Chuvil'deev, A. V. Nokhrin, M. M. Myshlyaev, V. I. Kopylov, et al., "Effect of recovery and recrystallization on the Hall-Petch relation parameters in submicrocrystalline metals: II. Model for calculating the Hall-Petch relation parameters," Russ. Metall. (Metally), No. 5, 487–499 (2018).
14. V. N. Chuvil'deev, A. V. Nokhrin, M. M. Myshlyaev, V. I. Kopylov, et al., "Effect of recovery and recrystallization on the Hall–Petch relation parameters in submicrocrystalline metals: III. Model for the effect of recovery and recrystallization on the Hall-Petch relation parameters," Russ. Metall. (Metally), No. 9, 867–879 (2018).
15. V. N. Perevezentsev, V. V. Rybin, and V. N. Chuvil'deev, "The theory of structural superplasticity. I. The physical character of the superplasticity phenomenon," Acta Met. Mater. **40** (5), 887–894 (1992).
16. V. N. Perevezentsev, V. V. Rybin, and V. N. Chuvil'deev, "The theory of structural superplasticity. III. Boundary migration and grain growth," Acta Met. Mater. **40** (5), 907–914 (1992).
17. V. N. Chuvil'deev, *Nonequilibrium Grain Boundaries in Metals. Theory and Applications* (Fizmatlit, Moscow, 2004).
18. V. N. Perevezentsev, O. E. Pirozhnikova, and V. N. Chuvil'deev, "Grain growth during superplastic deformation microduplex alloys," Physics of Metals and Metallography **71** (4), 29–36 (1991).
19. S. S. Gorelik, *Recrystallization of Metals and Alloys* (Metallurgiya, Moscow, 1967).
20. V. M. Segal, I. J. Beyerlein, C. N. Tome, V. N. Chuvil'deev, and V. I. Kopylov, *Fundamentals and Engineering of Severe Plastic Deformation* (Nova Sci. Publ., New York, 2010).
21. V. N. Perevezentsev, V. V. Rybin, and V. N. Chuvil'deev, "The theory of structural superplasticity. IV. Cavitation during superplastic deformation," Acta Met. Mater. **40** (5), 915–923 (1992).
22. V. N. Perevezentsev, V. V. Rybin, and V. N. Chuvil'deev, "Pore nucleation at the precipitate–matrix interface under superplastic deformation," Poverkhnost', No. 11, 130–139 (1986).

Translated by K. Shakhlevich